

N. G. Stefanis · S. V. Mikhailov · A. V. Pimikov

On the pion distribution amplitude.

Derivation, properties, predictions

Received: date / Accepted: date

Abstract We provide an in-depth analysis of the π distribution amplitude in terms of two different Gegenbauer representations. Detailed predictions for the $\pi - \gamma$ transition form factor are presented, obtained with light-cone sum rules. Various π distribution amplitudes are tested and the crucial role of their endpoint behavior in the form-factor analysis is discussed. Comparison with the data is given.

Keywords Pion distribution amplitude · platykurtic distribution · pion-photon transition

1 Introduction

The pion — the lightest meson — epitomizes the bound state of two light quarks within Quantum Chromodynamics (QCD). Employing light-front (LF) quantization, recently reviewed in [1], the n -parton wave function of the pion is defined in a frame-independent way by $\psi_{n/\pi}(x_i, \mathbf{k}_{\perp i}, \lambda_i)$. It is advantageous to consider instead, in lieu with QCD collinear factorization, the LF distribution amplitude (DA) [2], which is the LF wave function integrated over transverse momentum at fixed longitudinal momentum fraction $x_i = (k^0 + k^3)/(P^0 + P^3) = k^+/P^+$ of the pion's momentum P , with $\sum_{i=1}^n x_i = 1$. Then, the leading-twist-two DA of the $\bar{q}q$ valence state is described by $\varphi_\pi^{(2)}(x, \mu^2) = \int^{\mu^2} d\mathbf{k}_\perp^2 (16\pi^2)^{-2} \psi(x, \mathbf{k}_\perp)$. In operator language, this π DA is given by the following gauge-invariant matrix element:

$$\langle 0 | \bar{q}(z) \gamma_\mu \gamma_5 [z, 0] q(0) | \pi(P) \rangle |_{z^2=0} = i f_\pi P_\mu \int_0^1 dx e^{ix(z \cdot P)} \varphi_\pi^{(2)}(x, \mu^2), \quad (1)$$

where the gauge link $[z, 0] = \mathcal{P} \exp \left(ig \int_0^z A^\mu d\tau_\mu \right) = 1$ by virtue of imposing the lightcone gauge $A^+ = 0$. The momentum-scale dependence of the DA is controlled within perturbative QCD by a renormalization-group type evolution equation due to Brodsky, Lepage [2], and Efremov, Radyushkin [3] (ERBL). For this reason, one seeks to express the pion DA in terms of the eigenfunctions of this equation, i.e., the Gegenbauer harmonics $\psi_n(x) = 6x(1-x)C_n^{(3/2)}(2x-1)$ with the Gegenbauer

N. G. Stefanis
 Institut für Theoretische Physik II, Ruhr-Universität Bochum, D-44780 Bochum, Germany
 E-mail: stefanis@tp2.ruhr-uni-bochum.de

S. V. Mikhailov
 Bogoliubov Laboratory of Theoretical Physics, JINR, 141980 Dubna, Russia
 E-mail: mikhs@theor.jinr.ru

A. V. Pimikov
 Bogoliubov Laboratory of Theoretical Physics, JINR, 141980 Dubna, Russia
 E-mail: pimikov@theor.jinr.ru

polynomials $C_n^{(3/2)}(\xi = 2x - 1)$:

$$\varphi_\pi^{(2)}(x, \mu^2) = \psi_0(x) + \sum_{n=2,4,\dots}^{\infty} a_n(\mu^2)\psi_n(x), \quad (2)$$

where $\psi_0(x) = \varphi_\pi^{\text{asy}}(x) = 6x(1-x) \equiv 6x\bar{x}$ is the asymptotic DA and the nonperturbative content of the pion bound valence state is encoded in the expansion coefficients $a_n(\mu^2)$. Owing to the fact that the π DA (or any other hadron DA) is not directly measurable, one has to model it by determining the coefficients $a_n(\mu^2)$ at a typical hadronic scale of order $\mu^2 \sim 1 \text{ GeV}^2$ using some nonperturbative method (see next section) and use ERBL evolution to obtain them at any scale Q^2 . Regardless of the differences among these methods, the pion DAs share some particular properties which will be addressed in Sec. 3. In fact, the success or failure of a particular DA will depend on the ability to describe existing data for various pion observables and make tangible predictions for data to come (more in Sec. 4). Our findings will be summarized in Sec. 5, where we will also draw our conclusions.

2 Derivation of the π DA

The pion DAs used in our analysis were determined with the help of QCD sum rules with nonlocal condensates (NLC-SR for short) [4]. Our method derives from [5] in which the meson DA $\varphi_M(x)$ over the longitudinal momentum fractions $x \cdot P$ was linked to the distributions Φ_j of the virtuality of quarks and gluons in the nonperturbative vacuum of QCD. This was achieved by relating the pion and its first resonance A_1 to the correlator of two axial currents with NLC contributions in a sum rule:

$$f_\pi^2 \varphi_\pi(x) + f_{A_1}^2 \varphi_{A_1}(x) \exp\left(-\frac{m_{A_1}^2}{M^2}\right) = \int_0^{s_\pi^0} \rho_{\text{NLO}}^{\text{pert}}(x; s) e^{-s/M^2} ds + \frac{\langle \alpha_s GG \rangle}{24\pi M^2} \Phi_G(x; M^2; \Delta) + \frac{8\pi\alpha_s \langle \bar{q}q \rangle^2}{81M^4} \sum_{i=\text{S}, \text{V}, \text{T}_{1,2,3}} \Phi_i(x; M^2; \Delta). \quad (3)$$

Here the index i runs over scalar (S), vector (V) quark condensates, and quark-gluon condensates (T), while (G) denotes the gluon condensate. The most important parameter is the nonlocality $\Delta = \lambda_q^2/(2M^2)$, where M^2 is the Borel parameter and λ_q^2 is the average vacuum-quark virtuality, defined by $\lambda_q^2 = \langle \bar{q}igG^{\mu\nu}\sigma_{\mu\nu}q \rangle / 2\langle \bar{q}(0)q(0) \rangle \approx [0.35 - 0.45] \text{ GeV}^2$. This sum rule depends on the duality interval s_π^0 in the axial channel and involves the spectral density $\rho_{\text{NLO}}^{\text{pert}}(x; s)$ in next-to-leading order (NLO) of perturbative QCD [4; 6]. A whole family of admissible π DAs can be reconstructed [4; 7] from the above sum rule via the calculation of the moments $\langle \xi^N \rangle$ and also in terms of an independent sum rule for the inverse moment $\langle x^{-1} \rangle_\pi$:

$$\langle \xi^N \rangle = \int_0^1 dx \varphi_\pi^{(2)}(x, \mu^2) (2x-1)^N; \quad \langle x^{-1} \rangle_\pi = \int_0^1 \frac{\varphi_\pi(x)}{x} dx. \quad (4)$$

Below, we only summarize the main features of NLC-SRs, referring the reader for further details to [5; 4; 8]. (i) We start with the same condensates as in the standard (local) approach [9] but keep the nonlocal quantities $\langle \bar{q}(0)\Gamma q(z) \rangle$, $\langle G_{\mu\nu}(0)G_{\mu\nu}(z) \rangle$, etc. unexpanded. In this way, we obtain in Eq. (3) 6 functions Φ_j instead of 2 numbers for $\langle \bar{q}(0)\Gamma q(0) \rangle$, $\langle G_{\mu\nu}(0)G_{\mu\nu}(0) \rangle$. (ii) The nonlocal condensates are assumed to decrease with increasing distance (between vacuum fields). In fact, the *finiteness* of the widths of the NLCs plays a crucial role because it renders the RHS of Eq. (3) less singular in x [5]. To be specific, the singularities at the end points $x = 0, 1$, inevitable in the local approach, disappear. These finite widths have been estimated from the next higher terms in the expansions of the NLCs and are proportional to $\sim 1/\lambda_q^2$. (iii) To estimate the integral characteristics of $\varphi_\pi(x)$ in Eq. (4), it is plausible to approximate the NLC by Gaussian models which depend only on the single scale $\lambda_q^2/2$. This is sufficient to account for the main effect, i.e., the finite widths of the NLCs. The complete calculation of all NLO corrections to the RHS of the SR above will be undertaken in a separate work [10]. (iv) The evaluation of the SR in (3) enables us to estimate the first 5 moments $\langle \xi^{2,4,6,8,10} \rangle_\pi$ and, independently, the value of $\langle x^{-1} \rangle_\pi$. Making use of these estimates, a set of admissible pion DAs, was

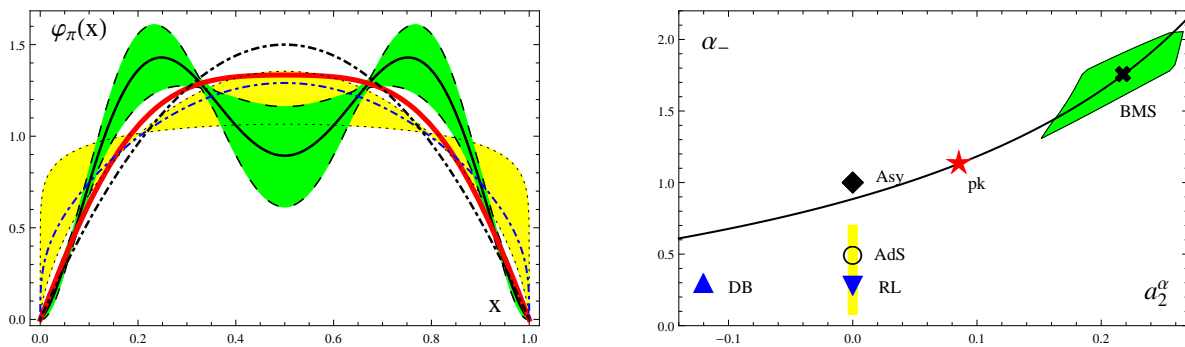


Fig. 1 *Left panel:* Pion DAs obtained within our NLC-SR method (dark-shaded green area), with the solid line inside it depicting the BMS DA [4]. The light-shaded yellow region of broad DAs shows the DSE results, the dashed-dotted line representing the DB DA [11]. The thick red line denotes the new platykurtic DA obtained in [10] and presented in [12]. *Right panel:* Pion DAs plotted in the (α_-, a_2^α) space. The curve denotes the orbit of DAs with the same value of $\langle x^{-1} \rangle_\pi \approx 3.13$. The normalization scale for both panels is $\mu^2 = 4 \text{ GeV}^2$.

determined in terms of 2 Gegenbauer harmonics [4; 8], which we display on the LHS of Fig. 1 in terms of a dark-shaded green area. The central curve within this band is termed the “BMS model” [4]. At the scale $\mu^2 \approx 1 \text{ GeV}^2$ it is given by $\{a_2^{\text{BMS}} \approx 0.2, a_4^{\text{BMS}} \approx -0.14\}$ using expansion (2).

Let us now turn our attention to another powerful method to extract the pion DA which is based on QCD’s Dyson-Schwinger equations (DSE) — see [13] for a general review and [14] for a review pertinent to the calculation of parton distribution amplitudes and functions for hadrons. The DSE-based derivation of the pion DA employs the determination of its first 50 $\langle x^n \rangle$ moments from which the pion DA is reconstructed in the form of the following Gegenbauer representation:

$$\varphi_\pi(x, \mu^2) = f(\{\alpha, a_2^\alpha, \dots, a_{j_s}^\alpha\}, x) = \psi_0^{(\alpha)}(x) + \sum_{j=2,4,\dots}^{j_s} a_j^\alpha(\mu^2) \psi_n^{(\alpha)}(x) \quad (5)$$

with $\psi_n^{(\alpha)}(x) = N_\alpha (x\bar{x})^{\alpha-} C_n^{(\alpha)}(2x-1)$, and $N_\alpha = 1/B(\alpha+1/2, \alpha+1/2)$, $\alpha_- = \alpha - 1/2$. Here α is considered to be a fit parameter and is not forced to the value $3/2$, i.e., to the conformal expansion. Two different procedures to treat the gap and the Bethe-Salpeter kernels in incorporating the nonperturbative features of dynamical chiral symmetry breaking (DCSB) were used in [11; 15], based on the rainbow-ladder (RL) truncation and the DCSB-improved (DB) kernel. The corresponding pion DAs are described by $\varphi_\pi^{\text{RL}}(x) = 1.74(x\bar{x})^{\alpha^{\text{RL}}} [1 + a_2^{\text{RL}} C_2^{(\alpha^{\text{RL}})}(x-\bar{x})]$ with $\alpha_-^{\text{RL}} = 0.29$, $a_2^{\text{RL}} = 0.0029$ and $\varphi_\pi^{\text{DB}}(x) = 1.81(x\bar{x})^{\alpha^{\text{DB}}} [1 + a_2^{\text{DB}} C_2^{(\alpha^{\text{DB}})}(x-\bar{x})]$ with $\alpha_-^{\text{DB}} = 0.31$, $a_2^{\text{DB}} = -0.12$. The profiles of the DAs, determined in [15] at the scale $\mu^2 = 4 \text{ GeV}^2$, are shown on the left panel of Fig. 1 in the form of the lower light-shaded yellow area within the range of errors on $\alpha_- = 0.35_{-0.24}^{+0.32}$ and $a_2^\alpha = 0$. This domain of α_- and a_2^α values incidentally includes the unrelated AdS/QCD model of [16] with $\psi_0^{(1)}(x)$ and $\alpha_- = 1/2$, depicted by an open circle on the right panel of Fig. 1. In order to compare our DAs with this sort of DAs, we switch from the conformal expansion (2) to the general expansion (5), employing the approximation of our DAs in terms of the lowest two terms a_2 and a_4 , viz.,

$$a_2 = \frac{7}{18} \int_0^1 dx f(\{\alpha, a_2^\alpha\}, x) C_2^{(3/2)}(2x-1); \quad a_4 = \frac{11}{45} \int_0^1 dx f(\{\alpha, a_2^\alpha\}, x) C_4^{(3/2)}(2x-1). \quad (6)$$

Solving this set of equations with respect to (α, a_2^α) , we get an approximate representation for each member of the BMS set of DAs, defined by (a_2, a_4) , in terms of (α, a_2^α) within the expansion Eq. (5) for $j_s = 2$. The result of this mapping for the whole BMS set of DAs is graphed on the right panel of Fig. 1 as a dark-shaded green area. The other depicted DAs are identified appropriately in the figure.

3 Properties of the π DA

As one sees from the left panel of Fig. 1, the profiles of the pion DA can vary significantly. Lattice simulations, while useful, can currently provide constraints only for the second moment $\langle \xi^2 \rangle$ (or equivalently the Gegenbauer coefficient a_2) [17; 18], while higher moments (coefficients) are still at large. Thus, lacking experimental evidence to restrict this variation, one may appeal to other *unbiased* tools to explore the structure of the pion DA. To this end, one of us has recently proposed [12] to use the Kuramoto model (see [19] for a review) which describes the synchronization of nonlinear oscillators in complex systems. The main features of Stefanis's approach are as follows. The longitudinal momentum fractions x are considered to be the natural frequencies (phases) of a large number ($N \rightarrow \infty$) of phase-coupled oscillators. The interaction among these oscillators gives rise to characteristic patterns of clustering in the interval $x \in [0, 1]$ which in turn correspond to particular DA profiles. The analysis in [12] has revealed that at finite momentum values of Q^2 , the x spectrum tends to synchronize as a result of nonperturbative correlations, encoded in nonlocal condensates, and the DCSB which is responsible for the generation of quark and gluon masses within a DSE-based framework. While the first effect suppresses the endpoints $x = 0, 1$, the DSE treatment yields strong enhancement of these regions. This contradicting behavior inspired in [12] the following parametrization of the pion DA $\varphi_\pi^{\text{true}}(x) \approx a\varphi_\pi^{\text{BMS}}(x) + (1-a)\varphi_\pi^{\text{DSE}}(x)$ with a mixing parameter $a \approx 0.7 - 0.9$.

Motivated by this finding, we furthered our NLC-SR-based approach and selected an admissible DA [10] that inherently combines the synchronization properties mentioned above and detailed in [12]. The profile of this DA, shown at the scale of 4 GeV^2 as a thick red solid line on the LHS of Fig. 1, is characterized by a broad maximum along a downward concave curve that bears a strong resemblance to the DSE DAs (DB and RL) over a large range of x values. However, its tails at $x = 0$ and $x = 1$ are suppressed, so that this DA has a platykurtic (pk) profile, in contrast to the family of the broad, endpoint-enhanced DSE DAs (light-shaded yellow band bounded by dotted lines on the LHS of Fig. 1). At the considered scale $\mu^2 = 4 \text{ GeV}^2$ it is given by $a_2^{\text{pk}} \approx 0.057$ and $a_4^{\text{pk}} \approx -0.013$ in terms of the conformal expansion in Eq. (2). Its position is marked on the right panel of this figure by the symbol \star at $(\alpha_- \approx 1.16, a_2^\alpha \approx 0.09)$. At the midpoint it gives $\varphi_\pi^{\text{pk}}(x = 1/2, \mu^2 = 4 \text{ GeV}^2) = 1.33$, which is close to $\varphi_\pi^{\text{RL}}(x = 1/2, \mu^2 = 4 \text{ GeV}^2) = 1.16$ and $\varphi_\pi^{\text{DB}}(x = 1/2, \mu^2 = 4 \text{ GeV}^2) = 1.29$ [11] and conforms well with the sum-rule estimate $\varphi_\pi(x = 1/2) = 1.2 \pm 0.3$ computed in [20]. Thus, the platykurtic DA can be interpreted as a realization of the Kuramoto-inspired parametrization proposed in [12]. As we will see in the next section, it leads to a prediction for the pion-photon TFF which is very close to that obtained with the original BMS DA.

4 Pion-photon transition and other π observables

Our predictions for $Q^2 F^{\gamma^* \gamma \pi^0}(Q^2)$ vs. Q^2 in comparison with the currently existing data [21; 22; 23; 24] are shown in Fig. 2 (left panel) in the form of a dark-shaded green band surrounded by a narrower blue one. The underlying DAs are the bimodal curves, obtained with NLC-SRs [4], within the dark-shaded band on the left panel. One observes that these predictions start to scale with Q^2 already at 10 GeV^2 . They are genuine state-of-the-art results because they comprise, within the framework of lightcone sum rules (LCSR), see, e.g., [25], *all* contributions to this TFF, currently known within QCD. These are: (i) NLO radiative correction, (ii) twist-four contribution, (iii) NLO ERBL evolution and (iv) quantified uncertainties related to the NNLO [26] and the twist-six corrections [27], as we detailed in [28] (inner wider green band), (v) the effect of a finite virtuality of the untagged quasi-real photon, included by employing the cut imposed in the Belle experiment ($q_2^2 \approx 0.04 \text{ GeV}^2$, see [7]) — narrow red strip below the outer band, while the effect of the extension of the BMS set to include in the analysis the $\psi_6(x)$ harmonic, leads [7] to the outer blue band. The root cause for the closeness of the calculated curves for the scaled pion-photon TFF with the bimodal BMS DA and the unimodal platykurtic DA can be traced to the fact that, for the leading twist contribution within the conformal expansion, one has $3/(\sqrt{2}f_\pi)Q^2 F_{\gamma^* \gamma \pi^0}^{(\text{LO})}(Q^2) = \langle x^{-1} \rangle_\pi = 3(1 + a_2 + a_4 \dots)$ [4; 29; 30], Hence, DAs with very different coefficients of the conformal expansion in Eq. (2) — and thus shapes — can nevertheless yield very close predictions for the pion-photon TFF, provided the corresponding inverse moment has similar values. In the case of the general expansion (5), one gets $\langle x^{-1} \rangle_\pi = [4\alpha/(2\alpha - 1)](1 + a_2^\alpha + \dots)$, so that the same effect appears for those DAs near the hyperbola shown on the RHS of Fig. 1.

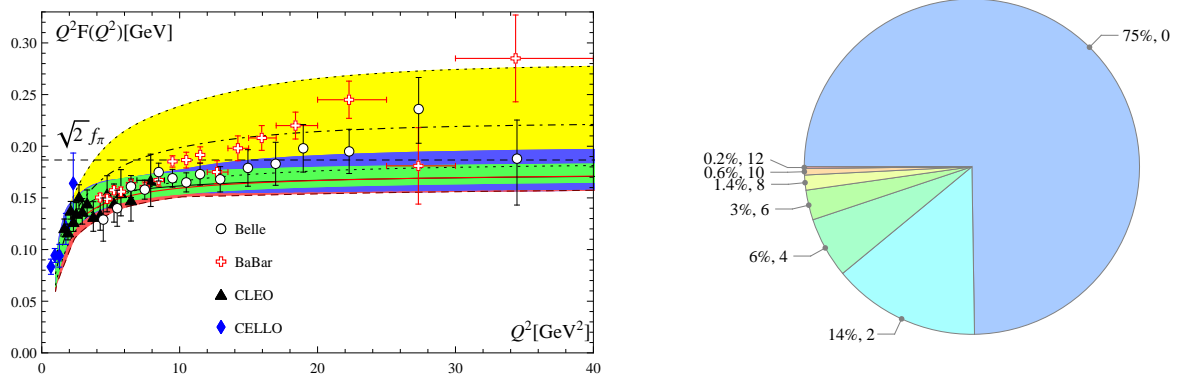


Fig. 2 *Left panel:* Predictions for $Q^2 F^{\gamma^* \gamma \pi^0}(Q^2)$ from our LCSR-based approach using as input BMS DAs [4] (lower, narrower green band) in comparison with the existing data and results we obtained with the DAs of the DSE framework [15] (upper, wider band bounded by dotted lines) by including the first ten coefficients a_n . The solid (red) line inside the inner shaded band shows the prediction obtained with the short-tailed platykurtic DA [10]. *Right panel:* Incremental inclusion of contributions to $Q^2 F^{\gamma^* \gamma \pi^0}(Q^2)$ stemming from the coefficients a_n from $n = 0$ up to $n = 12$ in the representation of the DB DSE DA for $\alpha_- = 0.35$ at the scale $Q^2 = 20 \text{ GeV}^2$.

The predictions obtained within our LCSR scheme for the pion-photon TFF, using as input the DSE DAs from [15], are graphed on the LHS of Fig. 2 in terms of the wider upper yellow band within the dotted lines. Inside this band the prediction due to the DB DA is depicted explicitly as a dashed-dotted line. Two observations are worth noting: First, the enlarged BMS band, which incorporates all mentioned contributions, overlaps with the DSE one along a narrow strip above $\sim 8 \text{ GeV}^2$. Second, the DB DA, favored in [11], obviously overshoots most experimental data in the whole Q^2 range. This discrepancy becomes more accentuated for the broader RL DA, obtained in [11] by imposing a rainbow-ladder truncation of the Bethe-Salpeter kernels in the DSEs. In this context we mention that the DA derived within a holographic AdS/QCD approach [16], notably, $\varphi_\pi^{\text{AdS/QCD}}(x) = (8/\pi)(x\bar{x})^{1/2}$ agrees better with the data relative to the DSE DAs (cf. the graphics on the RHS of Fig. 2 in Ref. [31]), the reason being that its endpoint regions are less pronounced. For similar reasons, the endpoint-concentrated Chernyak-Zhitnitsky DA [9] overshoots all data as well, see [28].

It is important to make some remarks on the computation of the above results. It was shown in [11] that the expansion in Eq. (5) provides a stable result already at $j_s = 2$, with $j_s = 4$ producing negligible changes. On the other hand, in order to include ERBL evolution, one has to go over to the conformal expansion of Eq. (2). The authors of [11] argued that one has to include terms of order $n \geq 14$ to ensure a stable conformal expansion of the pion DA. Though this may be right for the DSE DA, it is not necessarily true for the pion TFF calculated with it. Indeed, we investigated the rate of

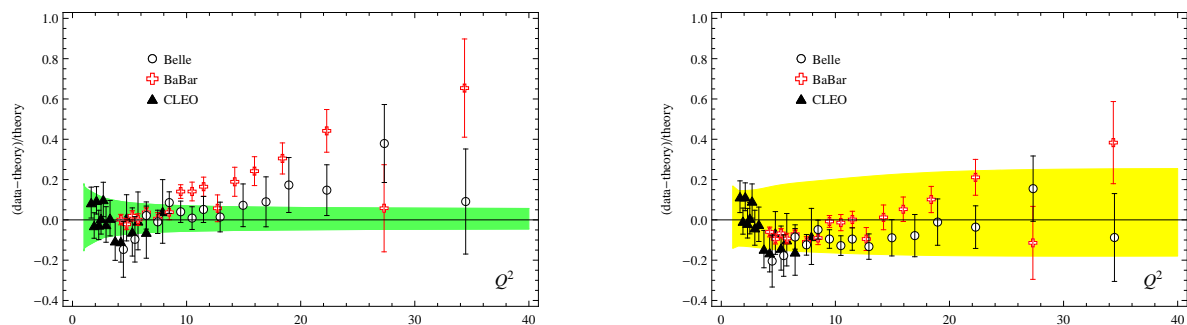


Fig. 3 (Data-Theory)/Theory vs. Q^2 . Theory (dark-shaded green area) is here our LCSR-based approach using as input the BMS DAs (bimodal and platykurtic) (left panel). The analogous illustration for the DSE DAs is shown in the right panel — wide yellow band. The computational technique is described in the text.

convergence of the pion-photon TFF, calculated within our scheme with the DSE DAs, quantitatively and found that already the contribution to the TFF stemming from the inclusion of the coefficient a_{12} plays only a marginal role (0.2%) — RHS of Fig. 2. Thus, our results obtained with the DSE DAs on the LHS of the same figure are unbiased predictions for $Q^2 F^{\gamma^* \gamma \pi^0}(Q^2)$ of the DSE approach.

To further quantify these statements, we plot in Fig. 3 the quantity (Data-Theory)/Theory against Q^2 , using as “Theory” our LCSR framework in connection with various DAs. The left panel of this figure shows the result for the bimodal BMS DAs (dark-shaded green strip), whereas the right panel displays the analogous graph for the DSE DAs light-shaded yellow band within the same scheme. The deviations of the high- Q^2 BaBar data from “Theory” with the BMS DAs are larger relative to those with the DSE ones. This is because the BMS predictions go approximately to a constant at high Q^2 as the lower band in the left plot in Fig. 2 reveals, while the DSE results (upper band) do not exclude an auxetic TFF behavior. In contrast, the platykurtic DA rules out a growth of the TFF and supports a scaling behavior at higher Q^2 . Note that model II, obtained with LCSRs in [27] and retrofitted to the Belle data in the second entry of [27], lies within the upper blue strip of our predictions.

Our NLC-SR-based pion DAs can be successfully used to describe other processes involving the pion DA. Examples are the pion elastic form factor [32], the diffractive di-jet production [30], and the meson-induced Drell-Yan production for the process $\pi^- N \rightarrow \mu^+ \mu^- X$ [33]. Two major findings of these analyses are worth mentioning here: (i) Using the convolution scheme developed in [34], it was shown in [30] that the derived predictions with the bimodal BMS DAs are in good agreement with the E791 di-jet events [35]— even in the central x region where the BMS DA “bunch” has its largest uncertainties (see left panel of Fig. 1). (ii) It was found in [33] that with the BMS DAs the angular parameters λ , μ , ν to describe the angular distribution of μ^+ in the unpolarized Drell-Yan $\pi^- N \rightarrow \mu^+ \mu^- X$ process comply best with the existing data.

5 Conclusions

We have presented detailed predictions for the pion-photon TFF which comprise all currently known QCD perturbative and nonperturbative contributions within a LCSR theoretical scheme. Within this scheme, we used several types of pion DAs as nonperturbative input on account of collinear QCD factorization. We found that BMS-like DAs, which are two-parametric bimodal distributions [4] replicate those data which are compatible with scaling, while they disagree with the high- Q^2 BaBar data which grow with the momentum. Crucially, this agreement is tightly connected to the endpoint behavior of these pion DAs and to much lesser extent to the broadness of the DA in the central region of x . Indeed, using QCD sum rules with nonlocal condensates, we determined a new DA which is a short-tailed platykurtic curve but leads to similar TFF results as the original BMS DAs. From the point of view of its profile, the platykurtic DA has a broadness similar to the DSE one, being downward concave, but has suppressed endpoint regions like the BMS DAs, thus somewhat “merging” these DAs, as argued in [12]. On the other hand, the predictions obtained within our framework with the endpoint-enhanced DSE-based DAs mostly overestimate the current TFF data. The distinct behavior of the presented forecasts — scaling vs. growth with Q^2 — for the pion TFF can serve to select the most appropriate model DA with the help of the expected Belle II data in the near future. Theoretically, it would be of great importance to explore in detail the relation of NLCs to the DSE framework.

Acknowledgements This work was partially supported by the Heisenberg–Landau Program (Grant 2014), the Russian Foundation for Fundamental Research under Grants No. 12-02-00613a and No. 14-01-00647, and the JINR-BelRFFR grant F14D-007.

References

1. Bakker, B.L.G., et al.: Light-Front Quantum Chromodynamics. Nucl. Phys. B (Proc. Suppl.) 251–252, 165 (2014)
2. Lepage, G.P., Brodsky, S.J.: Exclusive processes in perturbative quantum chromodynamics. Phys. Rev. D **22**, 2157 (1980)
3. Efremov, A.V., Radyushkin, A.V.: Asymptotical Behavior of Pion Electromagnetic Form-Factor in QCD. Theor. Math. Phys. **42**, 97 (1980)

-
4. Bakulev, A.P., Mikhailov, S.V., Stefanis, N.G.: QCD based pion distribution amplitudes confronting experimental data. *Phys. Lett. B* **508** (2001) 279; Erratum: *ibid. B* **590** (2004) 309
 5. Mikhailov, S.V., Radyushkin, A.V.: Nonlocal condensates and QCD sum rules for pion wave function. *JETP Lett.* **43** (1986) 712; Quark condensate nonlocality and pion wave function in QCD. *Sov. J. Nucl. Phys.* **49** (1989) 494; The Pion Wave Function And QCD Sum Rules With Nonlocal Condensates. *Phys. Rev. D* **45** (1992) 1754
 6. Bakulev, A.P., Mikhailov, S.V.: The rho meson and related meson wave functions in QCD sum rules with nonlocal condensates. *Phys. Lett. B* **436** (1998) 351
 7. Stefanis, N.G., Bakulev, A.P., Mikhailov, S.V., Pimikov, A.V.: Can We Understand an Auxetic Pion-Photon Transition Form Factor within QCD? *Phys. Rev. D* **87** (2013) 094025
 8. Bakulev, A.P., Mikhailov, S.V., Stefanis, N. G.: Deep inside the pion: Reconciling QCD theory with data. *Annalen Phys.* **13** (2004) 629
 9. Chernyak, V.L., Zhitnitsky, A.R.: Asymptotic Behavior of Exclusive Processes in QCD. *Phys. Rept.* **112** (1984) 173
 10. Mikhailov, S.V., Pimikov, A.V., Stefanis, N.G.: Work in progress
 11. Chang, L., et al.: Imaging dynamical chiral symmetry breaking: pion wave function on the light front. *Phys. Rev. Lett.* **110** (2013) 132001
 12. Stefanis, N.G.: What binds quarks together at different momentum scales? A conceptual scenario. *Phys. Lett. B* **738** (2014) 483
 13. Boucaud, P., et al.: The Infrared Behaviour of the Pure Yang-Mills Green Functions. *Few Body Syst.* **53** (2012) 387
 14. Cloet, I.C., Roberts, C.D.: Explanation and Prediction of Observables using Continuum Strong QCD: *Prog. Part. Nucl. Phys.* **77** (2014) 1
 15. Cloet, I.C., et al.: Pion distribution amplitude from lattice-QCD. *Phys. Rev. Lett.* **111** (2013) 092001
 16. Brodsky, S.J, Cao, F.G., de Teramond, G.F.: Evolved QCD predictions for the meson-photon transition form factors. *Phys. Rev. D* **84** (2011) 033001; Meson Transition Form Factors in Light-Front Holographic QCD. *Phys. Rev. D* **84**, 075012 (2011)
 17. Braun, V.M., et al.: Moments of pseudoscalar meson distribution amplitudes from the lattice. *Phys. Rev. D* **74** (2006) 074501
 18. Arthur, R., et al.: Lattice Results for Low Moments of Light Meson Distribution Amplitudes. *Phys. Rev. D* **83** (2011) 074505
 19. Strogatz, S.H.: From Kuramoto to Crawford: exploring the onset of synchronization in populations of coupled oscillators. *Physica D* **143** (2000) 1
 20. Braun, V.M., Filyanov, I.E.: QCD sum rules in exclusive kinematics and pion wave function. *Z. Phys. C* **44** (1989) 157
 21. Behrend, H.J., et al.: A measurement of the π^0 , η and η' electromagnetic form-factors. *Z. Phys. C* **49** (1991) 401
 22. Gronberg, J. et al.: Measurements of the meson photon transition form factors of light pseudoscalar mesons at large momentum transfer. *Phys. Rev. D* **57** (1998) 33
 23. Aubert, B., et al.: Measurement of the $\gamma\gamma^* \rightarrow \pi^0$ transition form factor. *Phys. Rev. D* **80** (2009) 052002
 24. Uehara, S., et al.: Measurement of $\gamma\gamma^* \rightarrow \pi^0$ transition form factor at Belle. *Phys. Rev. D* **86** (2012) 092007
 25. Khodjamirian, A.: Form factors of $\gamma^*\rho \rightarrow \pi$ and $\gamma^*\gamma \rightarrow \pi^0$ transitions and light-cone sum rules. *Eur. Phys. J. C* **6** (1999) 477
 26. Mikhailov, S.V., Stefanis, N.G.: Transition form factors of the pion in light-cone QCD sum rules with next-to-next-to-leading order contributions. *Nucl. Phys. B* **821** (2009) 291
 27. Agaev, S.S., Braun, V.M., Offen N., Porkert, F.A.: Light Cone Sum Rules for the $\pi^0 - \gamma^* - \gamma$ Form Factor Revisited. *Phys. Rev. D* **83** (2011) 054020; BELLE Data on the $\pi^0\gamma^*\gamma$ Form Factor: A Game Changer? *Phys. Rev. D* **86** (2012) 077504
 28. Bakulev, A.P., Mikhailov, S.V., Pimikov, A.V., Stefanis, N.G.: Pion-photon transition: The New QCD frontier. *Phys. Rev. D* **84** (2011) 034014; Comparing antithetic trends of data for the pion-photon transition form factor. *Phys. Rev. D* **86** (2012) 031501
 29. Bakulev, A.P., Mikhailov, S.V., Stefanis, N.G.: Unbiased analysis of CLEO data at NLO and pion distribution amplitude. *Phys. Rev. D* **67** (2003) 074012; Tagging the pion quark structure in QCD. *Phys. Rev. D* **73** (2006) 056002
 30. Bakulev, A.P., Mikhailov, S.V., Stefanis, N.G.: CLEO and E791 data: A Smoking gun for the pion distribution amplitude? *Phys. Lett. B* **578** (2004) 91
 31. Mikhailov, S.V., Pimikov, A.V., Stefanis, N.G.: Theoretical description and measurement of the pion-photon transition form factor. *Few Body Syst.* **55** (2014) 367
 32. Bakulev, A.P., Passek-Kumericki, K., Schroers, W., Stefanis, N.G.: Pion form-factor in QCD: From nonlocal condensates to NLO analytic perturbation theory. *Phys. Rev. D* **70** (2004) 033014
 33. Bakulev, A.P., Stefanis, N.G., Teryaev, O.V.: Polarized and unpolarized μ -pair meson-induced Drell-Yan production and the pion distribution amplitude. *Phys. Rev. D* **76** (2007) 074032
 34. Braun, V.M., Ivanov, D.Yu., Schäfer, A., Szymanowski, L.: Towards the theory of coherent hard dijet production on hadrons and nuclei. *Nucl. Phys. B* **638** (2002) 111
 35. Aitala, E.M. et al.: Direct measurement of the pion valence quark momentum distribution, the pion light-cone wave function squared. *Phys. Rev. Lett.* **86** (2001) 4768